

VIRUSES AND THEIR PENETRATION THROUGH FIBROUS STRUCTURES: A REVIEW

MILITKÝ, JIŘÍ* ; WIENER, JAKUB AND KŘEMENÁKOVÁ, DANA

Department of Material Engineering, Faculty of Textile Engineering, Technical University of Liberec, Liberec, Czech Republic

ABSTRACT

In the first part of this review the necessary information about structure and chemical composition of viruses are briefly discussed on the basic level. Main types of interaction of viruses with human cells are briefly described. The basic method of suppressing the spread of viruses from the surroundings of a healthy person and into the surroundings of an infected person is the use of protective equipment, especially face masks and respirators, where the active element is a fibrous structure. The protective functions of these structures depend on their composition (usually hydrophobic materials), construction (fabrics, knitted fabrics, non-woven fabrics, nano-meshes), morphology (porosity, thickness, pore distribution), the form of virus propagation (usually in water droplets as a type of aerosol), interaction conditions with the surface of the protective layer (speed of impact, conditions of capture on the surface of the fibrous phase, speed of penetration) and the method of virus inactivation (usually contact or very short-range interaction). It is therefore a very complicated problem that is often solved using a combination of mathematical modeling and simulation. The purpose is to present some methods of solving problems related to the protective function of fiber structures, which allow the specification of the suitability of these structures for real use.

KEYWORDS

SARS 2 virus structure; Viral attack; Filtration of droplets; Spreading on porous structures; Protective layers; Distribution of pore radii.

INTRODUCTION

The viruses are tiny organisms composed from many structural components influencing their penetration through fibrous materials and entering to human cells where it replicates. Especially the coronavirus SARS-CoV-2 is important because it is responsible for COVID pandemic. Coronavirus SARS-CoV-2 is composed from four types of structural proteins with different chemical composition and functionalities. Information about composition of this and similar viruses and modes of their interactions with human cells is advantageous for the creation of antiviral fibrous layers in face masks and antiviral clothing [1].

The wearing of face masks made of textile fabrics (generally referred to as "cloth masks") is likely to be a simple means of mitigating the transmission of Covid-19 (by preventing the transmission of contaminated droplets by an infected person) [2, 3]. Wearing a mask in public places and in the working environment is becoming part of everyday life. Face masks of type "Protecting your" are designed to provide sufficient filtration efficiency to stop the transfer of microdroplets ($\geq 5 \mu\text{m}$) from an infected

person to the environment [2]. Masks of the type "I protect myself" type are primarily intended for protection against the penetration of viruses and contaminated droplets from the environment [2]. In order to ensure the success of the functions of masks, the impact of various factors and influences that can avoid increase in the self-infection of an infected individual or create a path for secondary infection of uninfected subjects should be specified [3, 5]. There is no doubt that effective filtering ability and permeability of virus-containing droplets is a priority. The transparency of masks is also related to the loss of heat in the facial area, which plays an important role in the thermoregulation of the whole body [4]. Due to the high concentration of thermoreceptors, 20% of the total heat loss is cooling the skin [4].

The main aim of this review is to discuss problems related to the protective function of porous fibrous structures, and their interaction with water droplets transporting viruses. The structure of SARS 2 virus, basic mechanisms of interaction with human cells and spread by respiration into atmosphere are briefly discussed. Capture of droplets and particles by a fibrous layer (filtration) and their interaction with porous surfaces is predicted. Protective fibrous layers

* Corresponding author: Militký J., e-mail: jiri.militky@tul.cz

Received July 9, 2023; accepted August 23, 2023

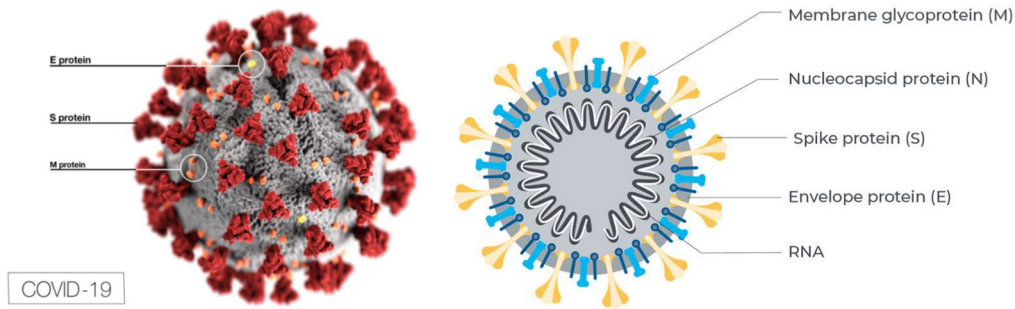


Figure 1. SARS-CoV-2 coronavirus (size 50–200 nanometers) (modified from [31, 32]).

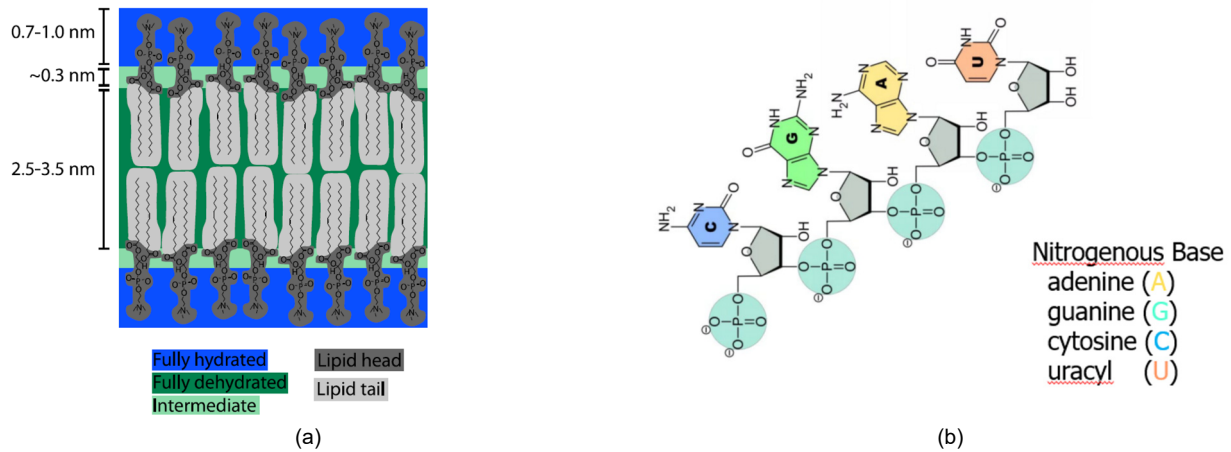


Figure 2. (a) Phospholipid bilayer (modified from [32, 33]), (b) Composition of RNA viruses (modified from [34]).

that are prepared for trapping viruses shown. There are mostly nano/micro assemblies prepared by electrospinning or non-woven textiles created by a combination of melt blown and electrospinning techniques. The pore size of these layers as tool for improvement of filtration characteristics active part of face masks are predicted.

SARS-COV-2 VIRUS

SARS-CoV-2 is a 50–200 nm globular RNA virus with an approximately spherical envelope and spikes (S-type proteins) that allow it to enter human cells where it replicates (Fig.1). It belongs to single-stranded RNA viruses with positive polarity. The coating, which is formed by a phospholipid bilayer (Fig. 2(a)), can be removed with alcohol or soap. The SARS-CoV-2 coronavirus (hereafter NKS, see Fig. 1) contains four structural proteins, known as S (tip), E (envelope), M (membrane) and N (nucleocapsid) [31].

The N-protein holds the RNA genome and the S, E and M proteins together form the envelope of the virus body. The S-protein is responsible for allowing the virus to attach to the host cell membrane. Chemically, they are primarily glycoproteins containing oligosaccharides covalently bound to the side groups of polypeptide chains. Bonds with glycoproteins of the virus are formed mainly by copper ions and the resulting complexes can prevent or strongly limit NKS replication in human cells [32, 35].

The RNA of coronaviruses is terminated at one end by a so-called "cap", which protects the viral RNA from the natural immunity of cells and degradation by cellular enzymes. At the other end, the viral RNA is terminated by a sequence of adjacent adenosine nucleotides (the so-called polyadenylate group). These modifications at both ends enable translation and increase RNA stability in cells. RNA is composed of ribose, which is a phosphate-type polysaccharide containing adenine, guanine, cytosine and uracil in the main chain (Fig. 2(b)). The O-H bond in RNA ribose makes the molecule more reactive. RNA is not stable under alkaline conditions and is susceptible to enzymatic degradation. RNA is constantly being produced, used, degraded and recycled. RNA is relatively resistant to UV damage.

It is highly desirable to solve the problem of masks preventing the penetration of NCS into the mouth and nose area of healthy persons (masks for prevention - RP) and masks preventing the spread of NCS from the mouth and nose area of infected persons (masks for the protection of the environment - RO).

INTERACTION OF VIRUSES WITH CELLS

Viruses are completely dependent on the cells they infect. These provide them with energy, metabolic intermediates and most (in some cases all) of the enzymes needed for their replication [35]). Viruses affect cells in a number of ways that can be divided into three partially overlapping categories:

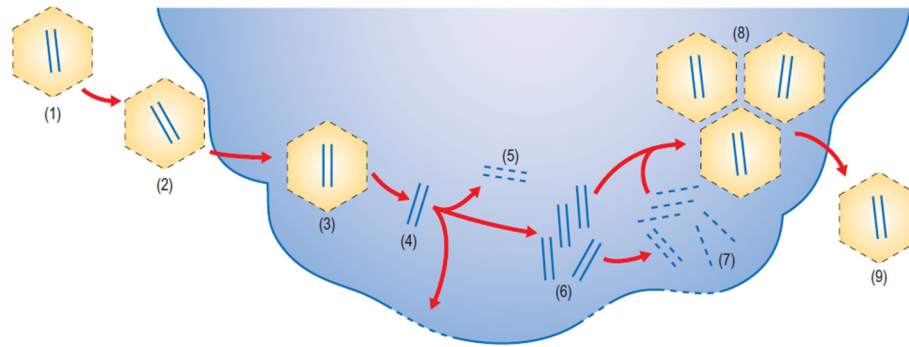


Figure 3. A simplified cycle of viral action where a hypothetical viral particle (1) attaches to the cell surface (2), enters the cell (3), is uncoated (4), undergoes temporal transcription and translation (5), then replicates the viral nucleic acid (6), final transcription and translation (7) and finally the assembly of new viral particles (8) and their release from the cell (modified from [35]).

1. Viruses that infect cells replicate within them and produce new virions that are released. This is the cytolytic cycle where the infection is productive and the cell culture exhibits cytopathic effects that are often characteristic of the infecting virus. In some cases, viruses are produced from infected cells, but the cells are not completely destroyed by the infection, so it is a non-cytolytic process that can become long-term.
2. Viruses that infect cells but do not complete the replication cycle. The infection is thus called abortive or non-productive. An abortive infection can be caused by a mutation of the virus, so that some basic function is lost, or defective interfering particles are produced, or interferons act. This may be possible in a steady state where infected and uninfected cells coexist and there is only limited virus production.
3. Viruses that do enter cells but are not produced by infected cells. The virus is maintained inside the cell in the form of DNA, which replicates in association with the DNA of the host cell. The host cell is called non-permissive and the infection is non-productive. Occasionally, this type of interaction leads to transformation, where the cell exhibits many of the characteristics of a tumor. In other cases, a latent infection follows, where the virus does not replicate and the cell retains its normal properties. First, there is contact and capture of viruses (adsorption) on the cell surface. The virus then enters the host cell and begins to replicate. The newly created virus particles are clustered and released (the diagram is in Fig. 3).

The basic parts of this cycle related to the possibilities of passivating the action of viruses by external means are their capture, penetration and release by replication.

Virus capture (adsorption)

The initial virus-cell interaction is a random collision and depends on the relative concentration of the virus. Under *in vitro* conditions, the ionic composition of the culture medium is important, when both viruses and cells are negatively charged and tend to repel

each other at neutral pH. The presence of cations such as Mg^{2+} helps promote contact. Adsorption then takes place via specific binding sites and receptors on the plasma membrane of the cell. It is largely a heat- and energy-independent process. Viruses vary greatly in the type of cells they can adsorb to, depending on the nature of the sites they can attach to. The presence of receptors determines whether the cell will be susceptible to the virus, but the cells must also be permissive: that is, for the successful production of new virions, they must contain a number of intracellular components that the virus needs for its replication. The ability of a virus to enter and replicate in a particular type of cell is called tissue or cell tropism. Many cell receptors are proteinaceous in nature, but they can also be composed of carbohydrates or lipids. The identification of receptors for specific viruses is very important because it facilitates antiviral therapy. The presence of a receptor molecule is required for most viruses to complete the entry phase of the replication cycle. There is probably a complex of interactions between different functional regions of viruses and receptors. These interactions often induce conformational changes in the surface proteins of the virus and form regions that are necessary for their penetration. Thus, the binding receptor may not be the only cause of tropism and the adsorption process may be influenced by factors such as virus strain, cell type, and even multiplicity of infection.

Entry of the virus into the cell (penetration)

Entry of the virus into the cell occurs immediately upon attachment and, unlike adsorption, requires energy and does not occur at $0^{\circ}C$. The speed of this phase of the replication cycle varies between different viruses, with some entering the cell in less than a second and others taking several minutes. Moreover, the efficiency of the process varies from roughly 50% of surface-attached viruses successfully entering the cell to less than 0.1%. In enveloped viruses, penetration occurs by membrane fusion catalyzed by fusion proteins in the viral envelope. Protein fusions that caused entry were divided into two categories.

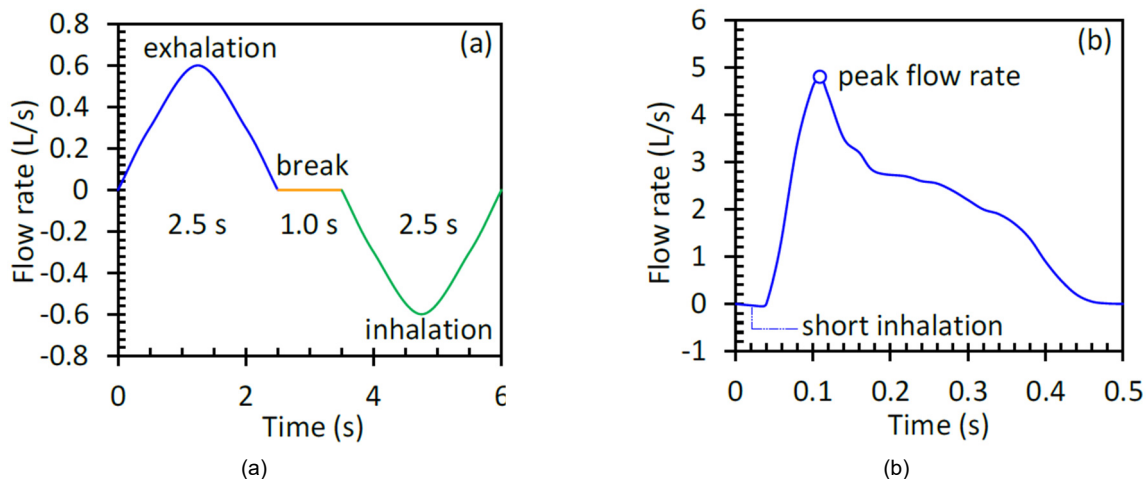


Figure 4. Accelerated breathing: (a) normal breathing process and (b) coughing process (modified from [18]).

Class I fusion proteins are trimeric spikes protruding from the surface of the viral particle and characteristically contain a fusion peptide composed of 20 hydrophobic amino acids. In some cases, such as HIV, fusion occurs in the cell at neutral pH with an activation energy ensuring receptor binding. In other cases, receptor-mediated endocytosis occurs.

Class II fusion proteins have distinct structural features and consist of heterodimers. Virus entry by endocytosis may be dependent on regions of the cell membrane that are rich in cholesterol and lipids. For many non-enveloped viruses, the mechanism of penetration through the host cell membrane in the absence of fusion is unclear. Recent findings suggest that such viruses can induce conformational changes in the membrane, resulting in the release of short membrane-interacting peptides. These break the membrane, allowing the virus to enter the cell.

Clustering and releasing replications

After the synthesis of viral proteins and viral nucleic acid, there is a replication assembly phase called morphogenesis. In general, the components that will form new virions are produced in large quantities and the assembly process is likely to be quite inefficient. This is followed by the release of replicated viral particles, i.e. the product of infection. Release is either through cell membrane rupture, as is typical of many non-enveloped viruses, or by penetration without cell destruction, as is typical of many enveloped viruses. Recently, some non-enveloped DNA viruses encoding a small basic regulatory protein (agnoprotein) whose function is to cause membrane permeabilization and subsequent release of newly synthesized viral particles have also been demonstrated. In some cases, viruses can be transferred directly from an infected cell to a neighboring cell, thereby avoiding any influence from the host's extracellular environment. Release without destruction of the cell membrane takes place by fusion of the viruses with the plasma membrane. The envelope of glycoproteins given by the type of virus is

synthesized by essentially the same mechanism as the cell membrane. The viral proteins to become the envelope contain a sequence of 15–30 hydrophobic amino acids known as the signal sequence. This sequence allows the virus to pass through the cell membrane. Up to several thousand replicating virus particles can be produced in a single infected cell, although this number varies widely with the type of virus and the type of host cell. The virus release process requiring membrane destruction is significantly faster. In general, few of the newly formed virus particles are infectious. Most probably they do not have the right composition of proteins, enzymes and nucleic acids, or are defective.

SPREAD OF VIRUSES

Viruses are generally spread by direct contact of people, animals and birds or indirectly by contact with contaminated surfaces, water, food and inhalation of contaminated air. Viral cores of respiratory droplets can remain suspended in the air for longer periods of time and be transported over longer distances by air currents. The mean free path of air molecules $\lambda = 72$ nm is very similar to the diameter of a virus, which increases the probability of molecular collisions. It is usually appropriate to also specify whether the spread of droplets occurs by breathing or coughing, as both processes have different kinetics (Fig. 4) [18].

Human breathing processes are highly dynamic (see Fig. 4). A typical breathing cycle includes a 2.5 s inhale, a 2.5 s exhale, and a 1 s hold. Within the respiratory cycle of an infectious airflow from an infected individual, only 2.5 s are exhaled during a 6 s cycle, while for an exposed individual there is still only 2.5 s inhalation of infectious airflows after a cleaning phase of 2.5 s exhalation and 1 s delay [18]. Lindsley et al. [11] measured the incidence of influenza virus in droplet nuclei produced by a coughing patient and reported that 42% of detected viruses were found in droplet nuclei <1 μm , 23% in droplet nuclei 1–4 μm , and 35% in droplet nuclei >4 μm . These dimensions determine the amount of

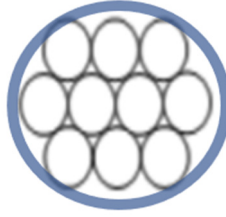


Figure 5. Idealized maximal honeycomb arrangement of a virus in a water droplet (blue envelope).

Table 1. Physical properties of water (see <https://www.britannica.com/science/water/Physical-properties>).

Dipole moment	2.95 ± 0.2 Debye
Boiling point	100°C at 101.325 kPa
Isothermal compressibility	0.4599 GPa ⁻¹
Density	997.05 kg/m ³
Dielectric constant	78.4
Diffusion coefficient	2.27×10 ⁻⁹ m ² /s
Enthalpy of vaporization	40.657 kJ/mol (100°)
Electronic polarizability (liquid)	1.48 Å ³
Specific heat capacity (C _p)	75.327 J/mol/K
Specific heat capacity (C _v)	74.539 J/mol/K
Thermal conductivity	0.610 W/m/K
Dynamic viscosity	0.8909 mPa·s

viruses that can be contained in one droplet. The diameter of a droplet enveloping closely spaced circular cross-section viruses can be predicted from idealized structural arrangements. A simple idealized model assumes of a limiting honeycomb arrangement of viruses in the cross-section of a water droplet. In a tight honeycomb structure, the viruses are ideally arranged in hexagonal concentric layers (Fig. 5).

In the first concentric layer of this structure there is only one virus, in the second layer there are 6 viruses and in the i -th layer ($i = 2, 3, \dots$) the number of viruses is equal to $n_i = 6(i - 1)$. The total number of ideally arranged viruses in l layers is equal to $n = 3l^2 - 3l + 1$. The number of layers l_n in a tight honeycomb structure is related to the total number of viruses n and the diameter of the aqueous envelope D_v . It holds that

$$l_n = 0.5 + \sqrt{\frac{n}{3} + \frac{1}{12}}, \quad (1)$$

and

$$D_n = 2d \left[\sqrt{\frac{n}{3} + \frac{1}{12}} - 0.5 + 1/(2 \cos 30^\circ) \right] \sqrt{3 \cos 30^\circ / \pi}, \quad (2)$$

where d is the diameter of the virus. From the knowledge of the size of the droplet and the diameter of the virus, it is possible to determine their theoretical maximum number in one droplet. In reality, the number of viruses will probably be much smaller. Most calculations and simulations apparently also use the idealized assumption that there is only one virus (diameter around 100 nm) in a spherical water droplet (diameter around 4 μm), so that the droplet

behaves like normal water droplets without a virus. A summary of the physical properties of water is given in Tab. 1

For an isolated water molecule (e.g., water in the gas phase), the HOH bond lengths are 0.095718 nm and the HOH bond angles is 104.474°. In the liquid state, both of these values are slightly modified by water-water and water-virus interactions. The dipole moment of one water molecule in the liquid state at 300 K is 2.95±0.2 Debye (1 Debye = 3.336×10⁻³⁰ Coulomb·m). The characteristics of respiratory flows, especially the speed and direction of exhalation flows, are strongly influenced by the geometry of the mouth and nose. The area of the mouth opening ranged from 100 mm² to 123 mm² during normal breathing, but exceeded 300 mm² during coughing. [12]. The total surface area of the nostrils during normal breathing varied widely, from 100 to 226 mm², and was predicted to be 330 mm² during coughing [12]. In real tests on humans, it was found that during coughing, the area of the mouth opening is 400 ± 95 mm² in men and 337 ± 140 mm² in women [13]. With regard to breathing mode, mouth-exhaled flow is important for both infected and exposed individuals [14]. Air flow exhaled through the mouth of an infected individual can easily penetrate the breathing area of a nearby individual. However, exhaled air flowing through the mouth of an exposed individual has a cleansing effect on the breathing area. Thus, the highest exposure is when the infected individual exhales through the mouth and the exposed individual exhales through the nose, while the lowest exposure is when the infected individual exhales through the nose and the exposed individual exhales through the mouth. Most computer fluid dynamics (CFD) studies simulate the “breath-only” mode for the

exposed individual and the “exhale-only” mode for the infected person [14, 15].

The well-known Wells-Riley model (see Eqn. 3) was developed to estimate the probability (P) of airborne transmission of an infectious agent in an indoor environment [16].

$$P = 1 - \exp\left(-\frac{I p q t_0}{Q}\right) d, \quad (3)$$

where I is the number of infected individuals, p is the respiration rate per person, q is the quantum rate of generation by the infected individual (quanta/s), that is the total exposure time t_0 , and Q is the outdoor air supply rate. The quantum is equal to the infectious dose. This model has been widely used to assess the risk of airborne cross-infection. Another characteristic is the reproduction number (RAO), which is the number of secondary infections that arise when there is one infected individual in a population in a shared indoor environment [17]

$$R_{A0} = (n - 1) \left[1 - \exp\left(-\frac{\bar{f} q t_0}{n}\right) \right], \quad (4)$$

where n is the number of people in the ventilated space and \bar{f} is the volume fraction of inhaled air that is exhaled by an infected person. The SARS-COV-2 virus primarily spreads through the air enveloped in water droplets [3]. It is mainly transmitted from infected persons by aerosol created by breathing and talking (up to 1.5 m), coughing (up to 2 m) or sneezing (up to 8 m). The droplet size ranges from 0.6 to 16 microns, but since it is a liquid, it can take any shape (the limit is the size of the virus) to allow penetration through porous hydrophobic materials. Air speed during inhalation and exhalation is around 80 km/h. When coughing and sneezing, it is up to 300 km/h. The volume of the lungs is about 5–6 liters [6]. Air consumption at different respiratory loads: at rest 8-10 l/min, walking 15-20 l/min, accelerated movement 20-30 l/min, medium load 30-40 l/min, high load 40-50 l/min, extreme load 50-120 l/min. It is therefore evident that the presence of aerosols containing viruses in the air leads to rapid infection without protection. Respiratory droplets can be of different

sizes and are commonly classified as aerosols (droplets that are smaller than 5 μm) and droplets (that are larger than 5 μm). Although the behavior of these droplets largely depends on environmental factors such as humidity, temperature, etc., in general, larger droplets settle due to gravity and do not spread over distances greater than 1–2 m. However, aerosols remain in the air for a longer time (due to their small size) and play a key role in the spread of infection. Due to ambient conditions, the water phase may evaporate or interact with impurities in the air, viruses may settle on these impurities and further spread on a solid surface or independently. Standard types of dirt such as dust and exhalation products are increasingly supplemented by micro- and nano-plastics [7,10], which, due to their hydrophobicity, can form surfaces on which viruses can be deposited. Due to their size and mass, droplets and aerosols settle under the influence of gravitational forces. It is known that the ratio between the sedimentation rate (proportional to d_p^2) and the Brownian motion (proportional to $d_p^{-1/2}$) changes due to the influence of the particle size d_p , as can be seen from Fig. 6.

If there is a situation where the viruses are alone in the air, they will settle down very slowly and therefore remain in the air for a long time. This situation occurs by removing the water phase either by evaporation (depending on the air temperature) or by contact with dirt in general and other surfaces. When evaluating the protective properties of fiber structures, a situation may arise when it is a liquid water particle containing a solid virus (the geometry changes easily) or when it is a solid particle with a surface-bound virus (the geometry does not change) with dimensions in the order of units of micrometers.

The virus is also transmitted by direct contact with the surfaces on which it is deposited. The virus can remain viable and infectious in aerosols for many hours and on surfaces (especially polymeric) for up to several days. So far, a practically unsolved problem is the limitation of virus attack from the surface of clothing textiles, especially due to direct infiltration by droplets spread from infected persons.

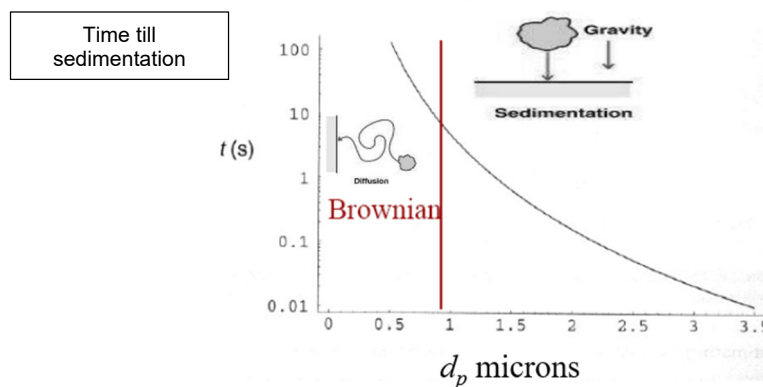


Figure 6. Effect of particle size on time to sedimentation.

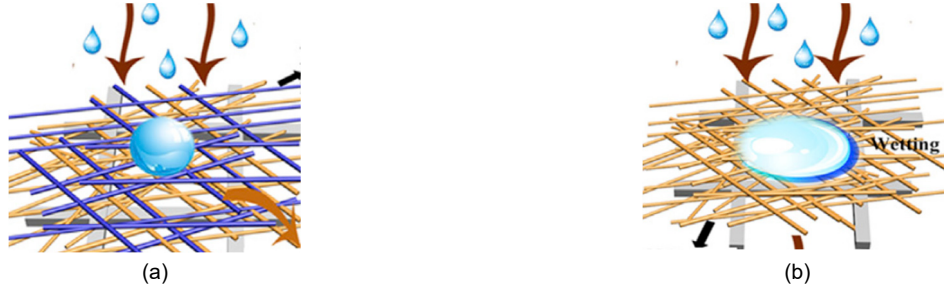


Figure 7. Water droplets on the surface of (a) hydrophobic fiber layers, (b) hydrophilic fiber layers (modified from [20]).

CAPTURE OF PARTICLES BY A FIBROUS LAYER (FILTRATION)

A mechanical protective layer capable of stopping the spread of the virus should ideally have pores smaller than the minimum size of the virus (from 50 nm), especially in the case of its small thickness (for continuous electrospun nanofibrous layers on Nanospider device, it is approximately 2 micrometers thick). The required pore size cannot be achieved using standard nanofibrous layers, where the pore size distribution is usually from nano to micrometers with a broad maximum in the region of several tens of microns. By further layering individual nanofibrous layers, it is possible to create a system with a much narrower pore size distribution [19]. In the case of larger material thicknesses, the curvature of the pores will play an important role, because viruses penetrating through can be deposited on the walls of the pores. Hydrophobic polymers are usually used as the material of the protective layer, when in contact with a porous surface spherical droplets are formed, which are more difficult to penetrate the pores (Fig. 7(a)) and are removed by movement over the surface.

On the other hand, the presence of hydrophilic fibers enables surface spreading of the droplets (Fig. 7(b)). In work [20], a new reusable two-layer fiber filter consisting of electrospun superhydrophobic poly(methyl methacrylate)/polydimethylsiloxane as a barrier for moisture penetration and super hydrophilic chitosan fibers for effective deposition of particles with high filtration efficiency was proposed. Surface interactions with water droplets influence the separation processes of viruses, which then behave as solid nanoparticles during filtration. The main mechanisms of filtration are therefore based on the removal of the carrier medium, capture and deposition, or absorption of particles. The removal of particles depends on the structure of the protective layer (fiber diameter, pore size and spatial distribution of fibers), particle size, air flow parameters (at the nanoscale it is practically exclusively laminar flow), etc. The capture mechanisms are mainly influenced by the size of the filtered particles. The mechanical mechanisms of particle contact with the fibers act as deviations of the particle trajectory from the air currents around the fibers

Inertial shock (impaction) is caused by the inertia of the particles and is the dominant process for relatively large particles that are unable to quickly adjust their direction to changes in the direction of the streamlines. In this case, the particles hit the surface of the fiber directly. Entrapment (interception) can occur when the particles are not far enough from the fiber surface and the particle radius is greater than the distance between the streamlines and the fiber surface. When the particle changes its original path due to sufficient kinetic energy sufficient for Brownian motion, chaotic diffusion begins, increasing the probability of contact with the fiber surface. Capture also occurs through electrostatic attraction between the particles and the filter medium. The mesh deposition mechanism is only relevant for particles whose size is larger than the filter pore size. For particles below 100 nm in size, random Brownian motion can drive the trajectory and capture is a consequence of random collisions with fibers. The primary mechanism of particle deposition on the surface of fibers is physical sorption, where intermolecular interactions between fibers and particles occur, such as van der Waals interactions, London interactions, hydrogen bonds, etc. The filtration efficiency due to Brownian diffusion η_d can be expressed by the relation [21]:

$$\eta_d = 1.6 \left(\frac{1 - \alpha}{K} \right)^{1/3} Pe^{-2/3}, \quad (5)$$

where $\alpha = 1 - \text{porosity}$, is packing density of the fibrous structure and

$$K = -\frac{1}{2} \ln \alpha - \frac{3}{4} + \alpha - \frac{1}{4} \alpha^2. \quad (6)$$

The Pecelt number Pe is defined as

$$Pe = \frac{U d_f}{D}, \quad (7)$$

where d_f is the fiber diameter, U is the air velocity and D is the diffusion coefficient

$$D = \frac{T k_B C_s}{3\pi\mu d_p}, \quad (8)$$

k_B is the Boltzmann constant, T is the absolute air temperature, μ is the dynamic air viscosity, d_p diameter of the diffusing particles and C_s is the Cunningham correction factor defined as

$$C_s \approx 1 + 2.52 \frac{\lambda}{d_p}, \quad (9)$$

where d is drop diameter and λ is the mean free path of the air ($\lambda = 0.072 \mu\text{m}$).

It can be seen that the filtration efficiency for capturing viruses (solid particles) is dependent on the, the diameters of the particles and the porosity of the protective fibrous layer.

INTERACTION OF PARTICLES WITH POROUS SURFACES

The physics of the impact of liquid droplets on surfaces depends on their type. There are two cases:

- a) the impact and spread of droplets on an impermeable substrate,
- b) impact and liquid penetration into the porous material due to impact energy and capillary forces.

When a drop hits a substrate, all of the drop's kinetic energy is converted to surface energy of the droplet deforming or dissipated by overcoming viscous forces. The relationship between the equilibrium contact angle θ_{eq} (formed by the droplet with the surface) and the surface tension is given by Young's equation $\gamma_{SV} = \gamma_{SL} + \gamma \cos(\theta)$, where γ_{SV} is the solid-gas surface tension (energy per unit area equivalent to force per unit length acting on the contact line), γ_{SL} is the solid-liquid surface tension and γ is the liquid-gas surface tension. Kinetic energy forces a liquid droplet to spread across a solid surface and also pushes it into pores in a permeable substrate. The droplet spreading kinetics can be expressed by the empirical Tanner model $R(t) = R_1 t^n$ where $R(t)$ is the

radius of the droplet at time t , R_1 is the radius of the droplet at time $t = 1$ s and n is a parameter dependent on the quantities significantly affecting the spreading process (viscosity, buoyancy, gravity, surface tension). A value of $n = 1/10$ was found for viscous spreading of small droplets. When a drop of diameter d hits a solid surface (especially hydrophilic, with a sharp contact angle), it spreads radially until it reaches a maximum spread D_m (see Fig. 8).

If the droplet does not break up, the droplet/substrate interaction can be divided into three phases: expansion, contraction, and equilibrium. These processes are illustrated in Fig. 9, where the ratio $D^* = D_m/d$ is plotted as a function of time.

The drop may shrink and after a few oscillations reach an equilibrium shape on the surface or it may spray and break up into small droplets or it may bounce off the surface. The final result of the drop impact depends on the impact speed of the drop, the size of the drop, the liquid and the properties of the surface including surface tension and surface roughness. To characterize the impact conditions, the Weber number is used:

$$We = \frac{\rho DV^2}{\gamma}, \tag{10}$$

where ρ is the density of the liquid (water), V is the impact velocity, D is the diameter of the droplet, γ is the surface tension, and μ is the viscosity of the liquid. To calculate the droplet expansion ratio D_m^* , the following relation can be used:

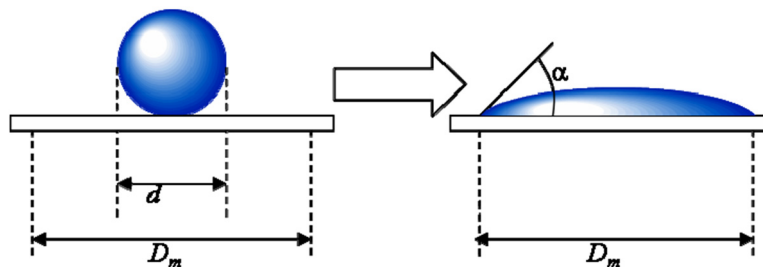


Figure 8. A drop of water on a hydrophilic surface (modified from [23]).

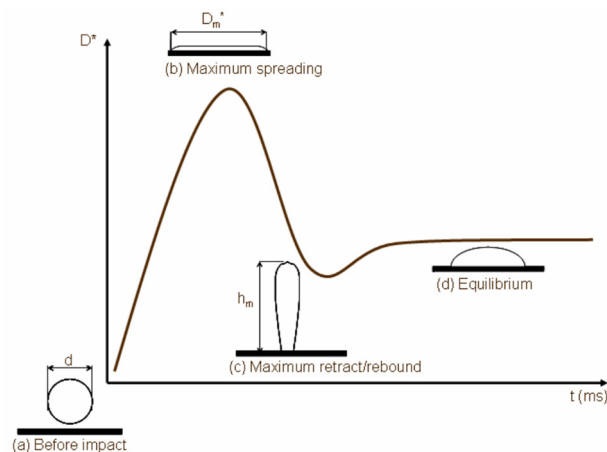


Figure 9. Phases of droplet interaction with a solid hydrophilic surface (modified from [23]).



Figure 10. Kinetics of spreading of water drops on polyester fabric: (a) time 2 s, (b) time 120 s and calculated contour.

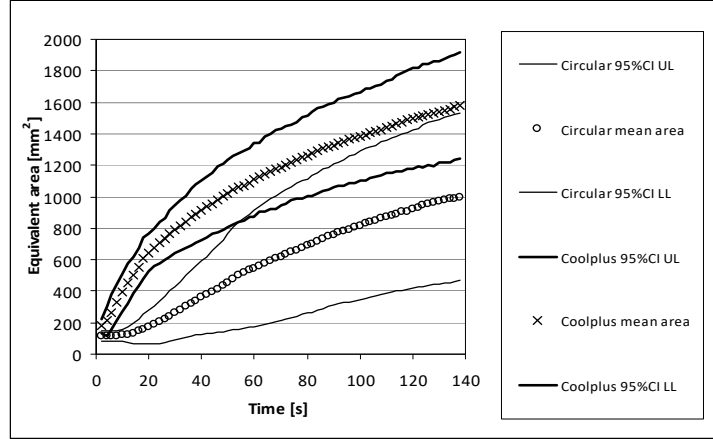


Figure 11. Dependence of equivalent areas on time, for "circular" and "Coolplus" samples.

$$D_m^* = 1 + 0.48W_e^{0.5} \exp[-1.48W_e^{0.22} R_e^{-0.21}], \quad (11)$$

where R_e is Reynolds number defined as:

$$R_e = \frac{VD\rho}{\mu}. \quad (12)$$

Whether the drop bounces or not depends on the ratio D_m^* and the equilibrium contact angle θ . The resulting equation for predicting this phenomenon has the form:

$$E_{ERE}^* = \frac{1}{4} \left(\frac{D_m}{d} \right)^2 (1 - \cos \theta) - 0.12 \left(\frac{D_m}{d} \right)^{2.3} (1 - \cos \theta)^{0.63} + \frac{2}{3} \left(\frac{D_m}{d} \right)^{-1} - 1. \quad (13)$$

The drop will bounce if E_{ERE}^* is greater than zero. At small R_e , the impact of a droplet on a solid surface results in its spreading (kinematic impact phase). The spreading radius of the droplet increases with time t according to the relation $R \sim t^{1/2}$ independently of the physical properties of the liquid and the surface. As R_e increases, droplet impact results in repeated reflections and especially splashing.

When studying the impact of drops on a porous substrate, its hydrophilicity, or hydrophobicity (characterized by $\cos \alpha$ or equilibrium contact angle θ) is manifested

As the porosity of the substrate increases, the liquid tends to penetrate more into the structure. An increase in porosity reduces the capillary pressure and reduces the force that draws liquid into the pores [22]. Increasing R_e increases the spreading rate of

droplets on the substrate surface, thereby shortening the time scale for penetration. At the same time, the inertia of the fluid penetrating into the porous substrate increases [22]. As Weber number We decreases, the effect of surface tension becomes more important. Capillary forces in the porous substrate increase, and a greater degree of penetration occurs. At the same time, the spread of the drop on the surface of the substrate is reduced due to the larger volume of liquid penetrating the substrate. Decreasing the value of the contact angle promotes wettability of the surface and greater penetration. The higher the wettability, the greater the liquid penetration, and the capillary pressure tends to draw the liquid more into the porous substrate. To monitor the kinetics of the spread of droplets on a porous surface, image analysis can be used, enabling the quantification of the outline of the droplets over time (see Fig. 10).

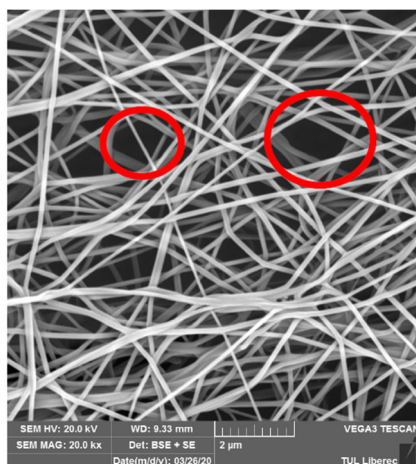
A MATLAB program (name DROP) was created to identify real contours. Equivalent perimeters P_i and areas S_i were calculated from contour coordinates. The equivalent radius of a spread water droplet RP_i based on the assumption that the real contour is replaced by a contour of a circular shape with the same circumference is given by the relation $RP_i = P_i/(2\pi)$ and the equivalent radius of a spread water drop RS_i assuming that the real contour is replaced by the contour of a circular shape with the same area, is calculated from the relation $RS_i = \sqrt{(S_i/\pi)}$. For illustration, Fig. 11 shows the time dependence of the equivalent areas of water drops on samples of

polyester textiles from Coolplus fibers and fibers with a circular cross-section.

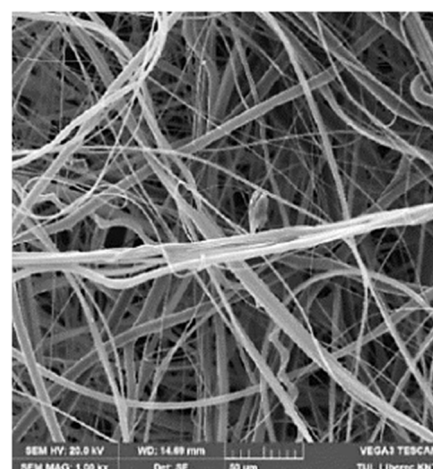
It has been confirmed that the cross-sectional shape of the fiber in the fabric has a significant effect on the kinetics of water droplet propagation due to microcapillary distribution. The ANSYS system and an idealized structure with regular cylindrical holes were used to simulate the spread of water droplets on the surface of a porous substrate associated with penetration into the pores. The results were compared with real structures containing regular cylindrical holes [22]. It was found that water droplets falling on a flat surface with small diameter drilled holes penetrated the holes on a time scale that was significantly longer than the droplet impact time. Liquid penetration into the holes was initially rapid, driven by the inertia of the impinging liquid. When the droplet reached its maximum extension and began to bounce, the inertia-driven motion was stopped. The subsequent flow of liquid into the holes was much slower, caused by capillary forces drawing the liquid in. A simple model accounting for fluid pressure, surface tension, and viscous forces predicted fluid velocity in both inertial and capillary-driven regimes [22].

PROTECTIVE FIBROUS STRUCTURES

Protective fibrous layers that are truly effective for trapping viruses are significantly different from conventional textile layers that trap liquid aerosols. These are mostly nano assemblies prepared by electrospinning (Fig. 12(a)) or non-woven textiles created by a combination of melt blown and electrospinning techniques (Fig. 12(b)) used for masks for prevention - RP and for masks for environmental protection – RO [2]. The improvement of filtration characteristics of these layers can be achieved by the appropriate choice of their structural parameters, which include fiber diameter, ratio of micro and nano fibers, thickness, porosity and areal mass.



(a)



(b)

Figure 12. Structures for face masks (a) classic nano mesh (b) combination of micro fibers and nano fibers (melt blown and nano mesh) [2].

A wide distribution of pore sizes is evident although the average pore size is acceptably small. To optimize such structures, the pore structure needs to be controlled, which includes not only the overall porosity and pore size distribution, but also their 3D shape and tortuosity. A number of experimental techniques such as scanning electron microscopy (SEM), pycnometer, mercury porosimetry, micro-computed tomography (micro-CT) [24] and, most recently, 3D confocal laser microscopy [25] are available to evaluate the pore structure.

Fig. 13 shows for illustration the procedure of analyzing the pore distribution from real SEM images of one nonwoven structure using the image analysis toolbox of the MATLAB program system. It uses adaptive thresholding (Otsu) and the regionprops() function.

The advantages and disadvantages of experimental approaches are examined in detail in [25]. Theoretical models can predict the pore structure of fiber structures with some morphological and structural parameters determined from real materials. For nanostructures forming short fiber sections, the average section length can also be easily determined experimentally and used in a geometric model.

The following idealized assumptions were used in the work [26] to construct the geometric model of the nanofiber entanglement:

1. All fibers (or fiber sections) are approximated as straight cylinders with diameter $d = \omega$ and length $l = \lambda$.
2. The probability that a point in the network plane has coverage c corresponds to the Poisson distribution.
3. The segments in the tangle of nanofibers are placed in arbitrary positions in the XY plane, neglecting the orientation in the direction of the Z axis.
4. The location of the fibers in the XY plane follows a Poisson random process.

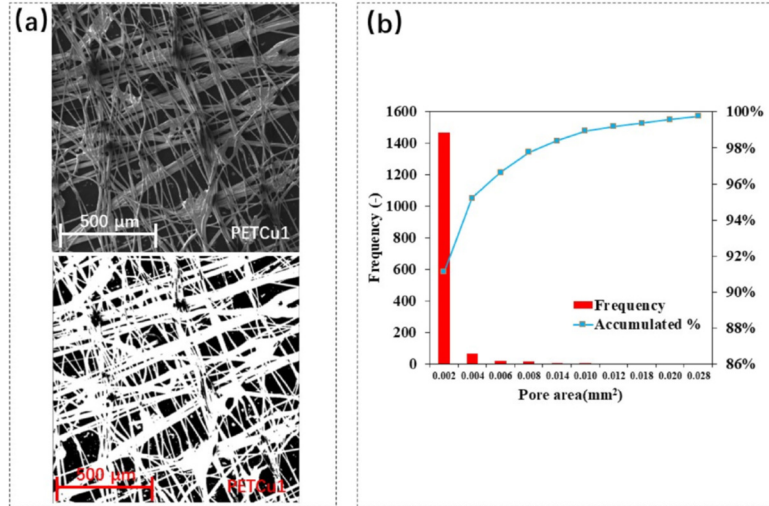


Figure 13. Pore distribution analysis (a) conversion of SEM image to binary image to display pore shape (b) pore size frequency plot.

By knowing the structural and morphological parameters of the nanofibrous structure, including the mean fiber diameter ω , porosity ε and thickness t , its expected average number of fiber contacts can be determined and the mechanical properties, pore size, and their distribution can be calculated. For mean value and variance of the pore radii in the elementary layer, the following relations can be derived [26]:

$$\bar{r} = \frac{\omega\sqrt{\pi}}{4} \left(\frac{1}{4 \log\left(\frac{1}{\varepsilon}\right)} + \frac{2A}{\pi} \right) \quad (14)$$

and

$$\delta^2(r) \left(\frac{1}{\pi} - \frac{\pi}{16} \right) \left[\left(\frac{1}{4 \log\left(\frac{1}{\varepsilon}\right)} + \frac{2A}{\pi} \right) \omega \right]^2, \quad (15)$$

here A is the ratio of the length and thickness of the fiber segments:

$$A = \frac{\lambda}{\omega}. \quad (16)$$

Assuming that the distribution of pore radii r in an elementary layer can be modeled using a gamma distribution, Sampson [27] derived the probability density and distribution function of the pore radius r in this layer:

$$f(r) = \frac{b^k}{\Gamma(k)} r^{k-1} e^{-br}, \quad (17)$$

where $\Gamma(k)$ is a gamma function with parameter k .

The probability density of pore radii in a nanofibrous structure formed by the superposition of n layers was derived assuming that each subsequent layer with independent and identical distribution of pore radii is placed over the previous layer such that the centers of the pore pairs in the layers are the same. For such a pair of layers, the radius of the smaller pore is assigned to each pair of pores. With this assumption, the probability density of the pore radii distribution of the multilayer nanofibrous assembly is:

$$f(r, n) = n \left(\frac{\Gamma(k, br)}{\Gamma(k)} \right)^{n-1} f(r), \quad (18)$$

where $\Gamma(k, br)$ is an incomplete gamma function with parameters k , br that can be determined from the

relations for mean value and variance of the pore radii:

$$\bar{r} = \frac{k}{b}, \quad \delta_x^2(r) = \frac{k}{b^2}. \quad (18)$$

The shape factor k characterizes the coefficient of variation CV of the pore radii in percent, i.e. $k = 1/CV^2$, where CV for random structures is usually $CV = \frac{1}{\pi} \sqrt{16 - \pi^2}$. A simple choice is $CV = 3$ based on approximate normality. The scale factor b is then simply calculated from the knowledge of the average pore radius from Eq. (19). To calculate the total porosity ε , a relationship based on the ratio of the density of the nanofibrous assembly (areal weight of the assembly divided by its thickness) and the density of the polymer forming the assembly is usually used.

In [28] was nanofibrous assembly simply assumed as solid straight rods having length L (usually more than 10 mm) diameter d and linear density J defined as:

$$\bar{r} = \frac{k}{b}, \quad \delta_x^2(r) = \frac{k}{b^2}. \quad (19)$$

The shape factor k characterizes the coefficient of variation CV of the pore radii in percent, i.e. $k = 1/CV^2$, where CV for random structures is usually $CV = \frac{1}{\pi} \sqrt{16 - \pi^2}$. A simple choice is $CV = 3$ based on approximate normality. The scale factor b is then simply calculated from the knowledge of the average pore radius from Eq. (19). To calculate the total porosity ε , a relationship based on the ratio of the density of the nanofibrous assembly (areal weight of the assembly divided by its thickness) and the density of the polymer forming the assembly is usually used. In [28] was nanofibrous assembly simply assumed as solid straight rods having length L (usually more than 10 mm) diameter d and linear density J defined as:

$$J = \frac{\pi d^2 \rho}{4}, \quad (20)$$

where ρ is (volumetric) density of fibrous elements. The nanofibrous assembly is characterized by porosity Po defined usually as:

$$Po = 1 - \frac{\rho h}{w}, \quad (21)$$

where h is nanofibrous assembly thickness and w is corresponding areal density. Let in this simplified nanofibrous assembly the location of nanofibrous segments centers follows Poisson process in two dimension and are independent each other. The orientation distribution of nanofibrous segments in selected direction is described by uniform distribution (in details see ([28])). The mean coverage Co of this nanofibrous assembly can be expressed by relation:

$$Co = \frac{wd}{J}. \quad (22)$$

The probability that a point in this nanofibrous assembly has coverage Co is given by the Poisson distribution with parameter Co . Under these assumptions is porosity related to mean coverage according to relation:

$$Po = \log\left(\frac{1}{Co}\right). \quad (23)$$

For porosities greater than 0.3, the mean pore diameter R_m of this nanofibrous assembly can be computed from relation:

$$R_m \approx \frac{\sqrt{\pi}}{4} \left(\frac{\pi}{2 \log\left(\frac{1}{Po}\right)} - 1 \right) d. \quad (24)$$

Based on these relations the nanofiber diameter and surface porosity of PAN nanofiber mats were studied ([29]). The results showed that increasing the PAN polymer concentration enhanced the nanofiber diameter but reduced the surface porosity of nanofiber mats. Because the diameter and in surface porosity are parameters that possess mutual effects, a structural parameter (Q) was introduced, and then its relation to some of the physical characteristics, such as the air permeability and surface roughness, was investigated. These simplified models can predict the pore structure and morphology of nanofibrous assemblies prepared by electrospinning. The mean pore diameter and probability density of penetrating particles size can be simply used for prediction of penetration of submicron creatures and as well drops containing viruses (see [30]).

CONCLUSION

The solution of problems related to the protective function of fibrous structures against the penetration of viruses and droplets containing also enveloping liquid water was shown. An overview of appropriate mathematical models and the results of some simulation studies were presented, which allow the assessment of the suitability of these structures for real use. Due to the complexity of the problem, the solution was restricted mainly by a combination of mathematical and stochastic modeling, and the simulation was limited only to strongly idealized situations. The MATLAB software system was used for image analysis and simple analytical models building. The various aspects of antiviral actions and their applications for construction of active fibrous

structures were published in book [1] and some articles [36-44] published in proceedings from conference TBIS devoted mainly to these topics.

REFERENCES

- Militký J., Prince A., Venkataraman M. (eds): Textiles and Their Use in Microbial Protection. Focus on COVID-19 and other viruses, London: CRC Press Boca Raton, 2021.
- Militký J., Novák O., Křemenáková D., et al.: A Review of impact of textile research on protective face masks, *Materials*, 14, 2021, 1937. <https://doi.org/10.3390/ma14081937>
- Gericke, A., Venkataraman, M., Militký, J.; et al.: Unmasking the mask: Investigating the role of physical properties in the efficacy of fabric masks to prevent the spread of the COVID-19 Virus, *Materials* 14(24), 2021, 7756. <https://doi.org/10.3390/ma14247756>
- Gericke, A., Militký, J., Venkataraman, M., et al.: The effect of mask style and fabric selection on the comfort properties of fabric masks, *Materials* 15(7), 2022, 2559. <https://doi.org/10.3390/ma15072559>
- Chua, M.H., et al.: Face Masks in the new COVID-19 normal: materials, testing, and perspectives. *AAS Research*, 2020, 7286735. <https://doi.org/10.34133/2020/7286735>
- Dobiáš J.: Determination of substances in exhaled air condensate, Diploma Thesis, Hradec Králové: UK Hradec Králové, 2006.
- Da Costa J.P., et al.: (Nano) plastics in the environment – sources, fates and effects, *Sci Total Environ*, 566–567, 2016, pp. 15–26. <https://doi.org/10.1016/j.scitotenv.2016.05.041>
- Da Costa J.P.: Micro- and nanoplastics in the environment: Research and Policymaking, *Current Opinion in Environmental Science & Health*, 1, 2018, pp. 12–16. <https://doi.org/10.1016/j.coesh.2017.11.002>
- Beaurepaire M., et al.: Microplastics in the atmospheric compartment, *Current Opinion in Food Science*, 41, 2021, pp. 159–168. <https://doi.org/10.1016/j.cofs.2021.04.010>
- Gasperi J., et al.: Microplastics in air: Are we breathing it in?, *Current Opinion in Environmental Science & Health*, 1, 2018, pp. 1–5. <https://doi.org/10.1016/j.coesh.2017.10.002>
- Lindsley W.G., et al.: Measurements of airborne influenza virus in aerosol particles from human coughs, *PLoS One*, 5, 2010, e15100. <https://doi.org/10.1371/journal.pone.0015100>
- Zhu S.W., et al.: Study on transport characteristics of saliva droplets produced by coughing in a calm indoor environment. *Build Environ.*, 41(12), 2006, pp. 1691-1702. <https://doi.org/10.1016/j.buildenv.2005.06.024>
- Gupta J.K., et al.: Flow dynamics and characterization of a cough, *Indoor Air.*, 19, 2009, pp. 517-525. <https://doi.org/10.1111/j.1600-0668.2009.00619.x>
- Villafuella J.M., et al.: Influence of human breathing modes on airborne cross infection risk, *Build. Environ.*, 106, 2016, pp. 340-351. <https://doi.org/10.1016/j.buildenv.2016.07.005>
- Liu L., et al.: Short-range airborne transmission of expiratory droplets between two people, *Indoor Air.*, 27(2), 2016, pp. 452-462. <https://doi.org/10.1111/ina.12314>
- Riley E.C., et al.: Airborne spread of measles in a suburban elementary school, *Am. J. Epidemiol.*, 107, 1978, pp. 421-432. <https://doi.org/10.1093/oxfordjournals.aje.a112560>
- Cermak R., Melikov A.K.: Protection of occupants from exhaled infectious agents and floor material emissions in rooms with personalized and underfloor ventilation. *HVAC&R Res.*, 13(1), 2007, pp. 23-38.
- Ai Z. T., Melikov A.K.: Airborne spread of expiratory droplet nuclei between the occupants of indoor environments: A review, *Indoor Air*, 28(4), 2018, pp. 500 – 524.

- <https://doi.org/10.1111/ina.12465>
19. Lee S., Obendorf K.: Use electrospun nanofiber web for protective textile materials as barriers to liquid penetration, *Textile Research Journal*, 77(9), 2007, pp. 696–702. <https://doi.org/10.1177/0040517507080284>
 20. Hui L., et al.: Transparent antibacterial nanofiber air filters with highly efficient moisture resistance for sustainable particulate matter capture, *iScience* 19, 2019, pp. 214–223. <https://doi.org/10.1016/j.isci.2019.07.020>
 21. Lee K.W., Liu B.Y.H.: Theoretical Study of Aerosol Filtration by Fibrous Filters, *Aerosol Sci. Technol.*, 1(2), 1982, pp. 147–161. <https://doi.org/10.1080/02786828208958584>
 22. Hosseini S.: Droplet impact and penetration on to the structured pore network geometries, PhD Thesis, Toronto: University of Toronto, 2015.
 23. Ok H.: Particle-laden drop impingement on a solid surface, PhD Thesis, Atlanta: Georgia Institute of Technology, 2005.
 24. Ho S.T., Hutmacher D.W.: A comparison of micro CT with other techniques used in the characterization of scaffolds, *Biomaterials* 27(8), 2006, pp. 1362–1376. <https://doi.org/10.1016/j.biomaterials.2005.08.035>
 25. Bagherzadeh R., et al.: Three-dimensional pore structure analysis of nanomicrofibrous scaffolds using confocal laser scanning microscopy, *J Biomed Mater Res Part A*, 101A, 2013, pp. 765–774. <https://doi.org/10.1002/jbm.a.34379>
 26. Bagherzadeh R., et al.: A theoretical analysis and prediction of pore size and pore size distribution in electrospun multilayer nanofibrous materials, *J Biomed Mater Res Part A*, 101A, 2013, pp. 2107–2117. <https://doi.org/10.1002/jbm.a.34487>
 27. Sampson W.W.: A multiplanar model for the pore radius distribution in isotropic near-planar stochastic fibre networks, *J Mater Sci*, 38, 2003, pp. 1617–1622. <https://doi.org/10.1023/A:1023298820390>
 28. Eichhorn J., Sampson W.W.: Statistical geometry of pores and statistics of porous nanofibrous assemblies, *J. R. Soc. Interface*, 2(4), 2005, pp. 309–318. <https://doi.org/10.1098/rsif.2005.0039>
 29. Borhani S., et al.: Structural characteristics and selected properties of polyacrylonitrile nanofiber mats, *Journal of Applied Polymer Science*, 108, 2008, pp. 2994–3000. <https://doi.org/10.1002/app.27904>
 30. Militký J., et al.: Penetration of mites through textile layer, In proceedings of: *Int conf. Medical textiles 96*. Bolton, 1996, https://en.wikipedia.org/wiki/Severe_acute_respiratory_syndrome_coronavirus_2
 31. https://en.wikipedia.org/wiki/Severe_acute_respiratory_syndrome_coronavirus_2
 32. Wu Z. et al.: Amino acid influence on copper binding to peptides, *J Am Soc Mass Spectrom.*, 21(4), 2010, pp. 522–533. <https://doi.org/10.1016/j.jasms.2009.12.020>
 33. Van Doremalen N., Bushmaker T., Morris D.H.: Aerosol and surface stability of HCoV-19 (SARS-CoV-2) compared to SARS-CoV-1, *MedRxiv*, 2020. <https://doi.org/10.1101/2020.03.09.20033217>
 34. Tinoco, I. et al.: How RNA folds, *Journal of Molecular Biology*, 293, 1999, pp. 271–81.
 35. Radke K., et al.: Viral interactions with the cytoskeleton: a hitchhiker's guide to the cell, *Cellular Microbiology*, 8(3), 2006, pp. 387–400. <https://doi.org/10.1111/j.1462-5822.2005.00679.x>
 36. Peng Q.-Y., Venkataraman M., Yang K., et al.: Kinetic model for disinfection with photo-oxidation. In: *Text. Bioeng. Informatics Symp. Proc. 2020 - 13th Text. Bioeng. Informatics Symp. TBIS 2020*, pp. 68-75, 2020.
 37. Faheem S., Militký J., Wiener, J.: Characterization, indication and passivation of SARS-CoV-2. In: *Text. Bioeng. Informatics Symp. Proc. 2020 - 13th Text. Bioeng. Informatics Symp. TBIS 2020*, pp. 76-83, 2020.
 38. Mahmood A., Militký J., Pechočiaková M., et al.: Eradicating spread of virus by photo-catalysis process. In: *Text. Bioeng. Informatics Symp. Proc. 2020 - 13th Text. Bioeng. Informatics Symp. TBIS 2020*, pp. 22-31, 2020.
 39. Wang D., Hu S., Kremenakova D. et al.: Virology of SARS-CoV-2, In: *Text. Bioeng. Informatics Symp. Proc. 2020 - 13th Text. Bioeng. Informatics Symp. TBIS 2020*, pp. 49-55, 2020.
 40. Hu S., Wang D., Yang K, et al.: Copper coated textiles for inhibition of virus spread. In: *Text. Bioeng. Informatics Symp. Proc. 2020 - 13th Text. Bioeng. Informatics Symp. TBIS 2020*, pp. 84-91, 2020.
 41. Tan X.-D., Peng Q.-Y., Yang K., et al.: Influence of UV light and ozonization on microbes, In: *Text. Bioeng. Informatics Symp. Proc. 2020 - 13th Text. Bioeng. Informatics Symp. TBIS 2020*, pp. 159-166, 2020.
 42. Khan M.Z., Militký J., Wiener J.: Enhanced disinfection of titanium dioxide, In: *Text. Bioeng. Informatics Symp. Proc. 2020 - 13th Text. Bioeng. Informatics Symp. TBIS 2020*, pp. 188-196, 2020.
 43. Karthik D., Militký J., Venkataraman M.: Eradicating spread of virus by using activated carbon, In: *Text. Bioeng. Informatics Symp. Proc. 2020 - 13th Text. Bioeng. Informatics Symp. TBIS 2020*, pp.56-63, 2020.
 44. Ali A., Militký J., Shahid M.: Copper based viral inhibition, In: *Text. Bioeng. Informatics Symp. Proc. 2020 - 13th Text. Bioeng. Informatics Symp. TBIS 2020*, pp.32-36, 2020.

This work is dedicated to prof. Izabella Krucińska from TU Lodz, who was not only a prominent scientific personality but also our close friend. A tribute to her memory.